Z. Phys. A – Atomic Nuclei 329, 243–254 (1988)

Zeitschrift für Physik A
Atomic Nuclei

Absolute Cross Section of the $^3He(\alpha, \gamma)^7Be$ Reaction*

M. Hilgemeier[1], H.W. Becker[1], C. Rolfs[1], H.P. Trautvetter[1], and J.W. Hammer[2]

[1] Institut für Kernphysik, Universität Münster, Münster, Federal Republic of Germany
[2] Institut für Strahlenphysik, Universität Stuttgart, Stuttgart, Federal Republic of Germany

Received October 12, 1987

The absolute cross section $\sigma(E)$ of the $^3He(\alpha, \gamma)^7Be$ reaction has been measured from $E_{c.m.} = 195$ to 686 keV. The studies employed both a supersonic jet gas target and an extended gas target, and were carried out by the observation of the prompt capture γ-ray transitions as well as the ^7Be residual nuclei. The absolute cross sections deduced from the capture γ-rays are in good agreement with most previous work and remove a discrepancy with other earlier work. In comparison, the $\sigma(E)$ values obtained from the ^7Be residual nuclei are systematically higher, suggesting a small production of additional ^7Be by contaminant reactions.

Nuclear Reaction: $^3He(\alpha, \gamma)$, $E_{c.m.} = 195$ to 686 keV; measured $\sigma(E)$; deduced astrophysical $S(E)$ factor. Windowless gas targets, beam calorimeter, Ge detectors.

PACS: 25.55.-e; 27.10; 27.20

1. Introduction

The absolute cross section $\sigma(E)$ of the $^3He(\alpha, \gamma)^7Be$ reaction is a key parameter in the solar-neutrino problem inasmuch as nearly all the neutrinos to which the Brookhaven solar-neutrino detector is sensitive are those arising from a branch in the $p-p$ chain involving this reaction [1–4]. Parker and Kavanagh [5] studied the reaction over a wide range of center-of-mass energies, $E = 180$ to 2500 keV, using a gas cell with a conventional entrance foil through which the incident beam had to pass. The γ-rays from the capture transitions were observed with NaI(Tl) crystals. The results for the astrophysical $S(E)$ factor,

$$S(E) = E\sigma(E) \exp(2\pi\eta) \quad (1)$$

with $2\pi\eta = 164.12/E^{1/2}$ (E in keV), indicated a somewhat steeper rise with decreasing energy than was suggested in the theoretical predictions based on the direct-capture (DC) model [6]. If the DC model prediction was matched to the whole data set, one arrived at an extrapolated $S(E)$ factor at zero energy of $S(0) = 0.47 \pm 0.05$ keV-b. Subsequently, the measurements were extended [7] to lower energies ($E = 164$ to 245 keV) using a windowless gas target to minimize energy loss and energy straggling of the beam. The capture γ-rays were detected with NaI(Tl) crystals. The combined results were fitted by a polynomial, leading to $S(0) = 0.61 \pm 0.07$ keV-b [7]. However, a reanalysis of both data sets separately, guided by the DC model predictions, leads to a mean value of $S(0) = 0.52 \pm 0.05$ keV-b [4, 8]. More recently, data have been obtained [9] as low as $E = 107$ keV using high-resolution Ge(Li) detectors in combination with windowless gas targets, including a quasi-point supersonic jet. The observed γ-ray angular distributions for the capture transitions into the ^7Be ground state (DC $\rightarrow$ 0) and 429 keV first excited state (DC $\rightarrow$ 429), the energy dependence of their intensity ratio, as well

* Supported in part by the Deutsche Forschungsgemeinschaft (Ro429/15-2)

as the energy dependence of the total $S(E)$-factor data were in excellent agreement with the DC model calculations. Thus, the agreement with the DC model over a wide range of energies supports its use in extrapolation of the data to zero energy. Using the DC model [6], the extrapolation of the data led to $S(0)=0.32\pm0.04$ keV-b (or 0.30 keV-b using other models [9]). Other recent measurements [10], using similar experimental techniques, confirmed the energy dependence of the branching ratio and of the $S(E)$ factor; however, a discrepancy of about 40% in the absolute values remained. The higher absolute values [10] were subsequently confirmed for a slightly higher energy region [11, 12], by measuring the delayed ^7Be radioactivity induced by the bombardment (activation technique). The extrapolated absolute $S(0)$ factor, arrived at using only the higher values, is $S(0)=0.52\pm0.02$ keV-b [4]. It was however pointed out [13] that all of the prompt γ-ray measurements appear to converge at $S(0)=0.50\pm0.02$ keV-b, while measurements using the activation technique [10–12] are systematically higher by about 16% ($S(0)=0.58\pm0.02$ keV-b).

The absolute cross sections reported by Kräwinkel et al. [9] were derived predominantly from the measurements using a quasi-point supersonic jet gas target (8 of 11 cases, Table 3 of [9]). A crucial quantity in these measurements is the number of target atoms (N_t, in units of atoms per unit area) in the jet target zone. Due to the pointlike nature of these jet gas targets (about 2 to 3 mm diameter, [14, 15]), it was found subsequently [16, 17] that the overlap of the ion beam profile with the gas density profile is extremely critical for absolute cross section measurements and depends on the characteristics of the incident ion beam, the precision in alignment and the size of the beam-defining collimators. This is the case in particular for the light gases hydrogen and helium. In situ measurements of this overlap are thus of utmost importance in absolute cross section measurements, which could otherwise lead to systematic errors. For example, in the work of Kräwinkel et al. [9] the number of ^3He and ^4He jet target atoms N_t was measured via elastic scattering yields and via energy loss data (Table 2 of [9]), where the first method led to N_t values a factor 1.4 smaller than the adopted values. On the basis of these smaller N_t values, the absolute $S(0)$ value derived from the jet-target measurements would increase to 0.45 ± 0.06 keV-b, consistent with the other $S(0)$ values quoted above. Thus, it is suggested that the helium gas density of the supersonic jet was actually lower than the values used in the previous analyses of Kräwinkel et al. [9], and that correcting the gas density to the value indicated by the elastic scattering essentially removes the discrepancy.

The present work describes efforts to test this suggestion. Measurements using a quasi-point jet gas target are described in Sect. 2 and those using an extended gas target in Sect. 3. In both cases the prompt capture γ-rays of the $^3He(\alpha,\gamma)^7Be$ reaction are observed with an intrinsic Ge detector. The resulting γ-ray yield $I_\gamma(E)$ is related to the cross section $\sigma(E)$ via the expression

$$I_\gamma(E)=N_p\, n_t\, l_{\text{eff}}\, \varepsilon_\gamma\, W(\theta_\gamma, E)\, \sigma(E), \tag{2}$$

where N_p is the number of incident projectiles, n_t the number of target atoms per unit volume, l_{eff} the effective target length seen by the γ-ray detector ($N_t = n_t\, l_{\text{eff}}$), ε_γ the absolute γ-ray efficiency and $W(\theta_\gamma, E)$ the known angular distributions [5, 6, 9]. Although the setups in both cases are similar to those described previously [9], they have been improved in several details (e.g., geometrical arrangements) to allow for a higher precision in the determination of the quantities N_p, n_t, l_{eff} and ε_γ. Section 4 describes concurrent measurements of the capture γ-ray transitions and of the ^7Be residual nuclei (via their electron capture decay to ^7Li). Finally, the results are compared with previous work in Sect. 5. Details of all aspects of this work beyond those reported in this paper can be found in [18].

2. Measurements Using the Supersonic Gas Jet Target

2.1. Experimental Equipment and Setup

2.1.1. Accelerator. The 350 kV accelerator at the Institut für Kernphysik in Münster provided beams of $^1H^+$, $^3He^+$ and $^4He^+$ ions at energies $E_{\text{lab}}=275$ to 352 keV with particle currents of up to 130 μA at the target. The ^3He gas in the terminal of the accelerator was recirculated. The energy calibration of the accelerator facility [19] has been checked during the course of the experiments and is known to better than ±0.3 keV [18].

2.1.2. Jet Gas Target System. The quasi-point supersonic gas jet target (Fig. 1a) has been described elsewhere [14, 15]. Briefly, the target gas at an inlet pressure p_0 (here: ^4He gas at 1.96 ± 0.04 bar) flows through a Laval nozzle (1 mm diameter at the neck) and, after free expansion over a path of 6.0 mm, the jet stream is mostly captured by a receiver pumped by a Roots blower. The jet assembly is placed in a cylindrical target chamber (40 cm diameter, 18.5 cm height), in which the pressure p_t is several orders of magnitude lower (here: $p_t=0.49\pm0.03$ mbar) than the inlet pressure, thus forming a geometrically confined

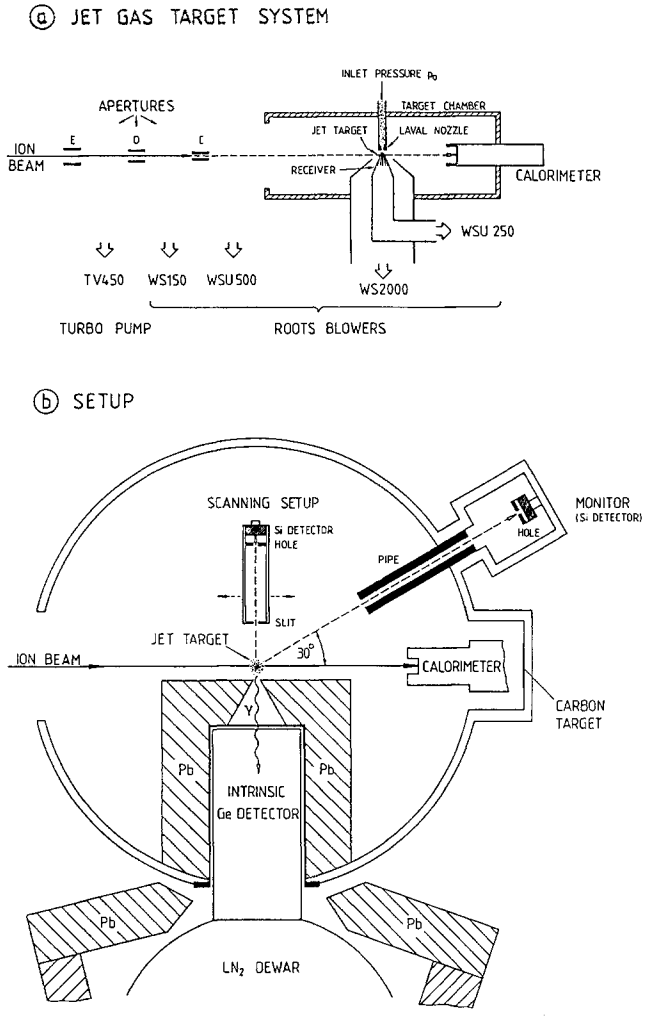

Fig. 1a and b. Schematic diagram of **a** the jet gas target system and **b** the setup in the target chamber. The beam axis is defined by the aperture *C* (3 mm diameter) in front of the jet target. The target gas flowing through the Laval nozzle is pumped differentially with the use of Roots blowers and a turbopump

supersonic jet stream. In this arrangement, the high density region in the supersonic jet near the outlet of the nozzle is chosen as the target zone (3.0 ± 0.3 mm distance from the nozzle) and this jet target zone can be seen from every scattering direction. For optimum alignment of the Laval nozzle with regard to the receiver, the nozzle is placed on a device [18] allowing in situ adjustment of the nozzle (± 8 mm) in all directions. The gas outside the target region is pumped differentially using Roots blowers and a turbo pump (Fig. 1a). The gas compression up to the inlet pressure p_0 is achieved with a combination of Roots blowers and metal bellows compressors [14]. The gas pressure at the inlet of the Laval nozzle as well as in the target chamber is measured with Baratron capacitance manometers to an accuracy of better than 4%. The pressure measurement with these manometers is absolute and independent of the type of gas used. Reduction of gas pressure along the beam axis, due to beam induced heating, is less than 5% for the 1.96 bar inlet pressure used and the 130 μA maximum beam current employed (for details, see [20]). The cleaning elements used in the gas recirculation system have been described previously [14]. A zeolite adsorption trap at liquid nitrogen temperature was very efficient for the cleaning of the helium target gas (chemical purity of better than one part in 10^6). The gas composition was monitored with a *Q*200 mass spectrometer.

2.1.3. Jet Target Chamber and Setup. A schematic diagram of the relevant parts of the jet target chamber and of the experimental setup is shown in Fig. 1b. The beam enters the chamber through a 3 mm diameter aperture (*C*), passes through the jet gas target at the center of the chamber (at a distance from the aperture of 310 ± 2 mm) and is stopped in a 200 W calorimeter (Sect. 2.1.4). In other experiments, the calorimeter was replaced by a ^{12}C target on a Ta backing (distance to the jet target $=262\pm2$ mm), where the target substrate was directly watercooled. The target chamber has several ports which are used for various purposes.

In order to obtain information on the radial density distribution of the supersonic jet stream at the selected target area (near the outlet of the Laval nozzle), a proton beam of $E_p=352$ keV was incident on the jet target zone (with a beam diameter of less than 1 mm) and its elastic scattering yield was observed at $\theta_{lab}=90°$ in a 300 μm thick Si detector (active area $=25$ mm^2) placed in a scanning setup (Fig. 1b). The detector was collimated by a circular aperture (area $=0.116\pm0.003$ mm^2, as determined with a calibrated α-source) and a 20 mm high slit aperture (slit-width $=0.30\pm0.01$ mm) placed at respective distances from the jet target of 118.7 ± 0.6 mm and 39.5 ± 0.5 mm. In this setup the detector views a horizontal length of $l=0.45$ mm over the jet target zone, leading to the product $\Delta\Omega\times l=(3.70\pm0.17)\times10^{-7}$ sr−cm. The detector arrangement can be shifted parallel to the beam direction (with a precision of ±0.01 mm), whereby the elastic scattering yield traces the radial density distribution in the jet target zone along the beam axis. The relative number of incident projectiles was monitored in these measurements via the elastic scattering yield observed with a monitor detector at $\theta_{lab}=30°$ (Sect. 2.1.4). The results for ^4He gas at the inlet pressure $p_0=1.96$ bar are illustrated in Fig. 2 and yield a FWHM jet width of $l_j=2.0\pm0.1$ mm, in good agreement with previous work [14].

The capture γ-ray transitions were observed in a 145 cm^3 intrinsic Ge detector, with an energy resolution in the setup of 2.0 keV at $E_\gamma=1.33$ MeV. A 4 mm

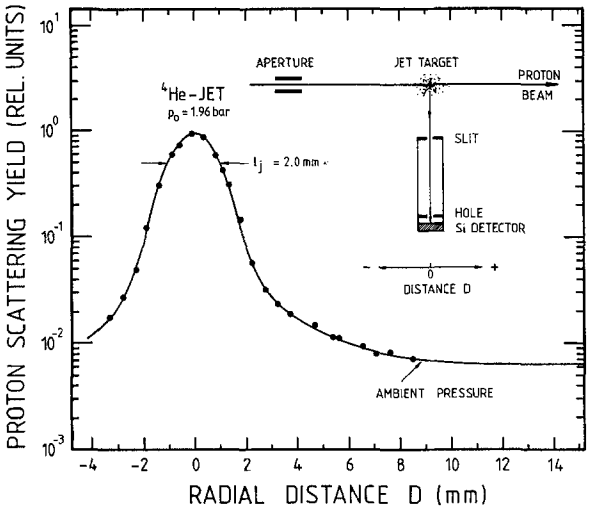

Fig. 2. Radial density distribution of the supersonic jet stream at the selected target area (near the outlet of the Laval nozzle) is shown for ^4He gas at an inlet pressure of $p_0 = 1.96$ bar. The data have been obtained via proton elastic scattering ($E_p = 352$ keV) as observed in a scanning setup (inset). The density distribution drops steeply (factor of 120) at the edge of the supersonic jet stream to the ambient pressure in the target chamber. The curve through the data points is to guide the eye

thick Al port at the target chamber (Fig. 1b) allowed one to install the Ge detector at $\theta_\gamma = 90°$, with its front face at a distance of 5.7 ± 0.1 cm from the jet target. The Ge detector was surrounded by a lead shield (4.5 cm thickness for the side blocks, 3.0 cm thickness for the blocks on the top and the bottom of the detector housing, 5.0 cm thickness elsewhere), whereby the room background was suppressed by 85%. The front face of the lead shielding had a 12 mm diameter hole with a conical shape (angle = 56°) allowing the Ge detector to see the full jet target zone and minimizing γ-ray yield contributions from regions outside the jet target zone. In other experiments (Sect. 2.2.3), the Ge detector was placed at $\theta_\gamma = 0°$ in close geometry to the ^{12}C target.

2.1.4. Current Measurement. Charge exchange effects of the incident ion beam in the gas before striking the Faraday cup make a reliable charge integration difficult if not impossible. Instead, the elastic scattering yields of the beam particles on the gas target nuclei in the supersonic jet system were observed in a Si detector (monitor) placed at $\theta_{lab} = 30°$. The detector was collimated (Fig. 1b) with a circular aperture (area $= 0.0264 \pm 0.0012$ mm^2, as determined with a calibrated α-source) at a distance of 269 ± 2 mm from the jet target and a pipe of 6 mm inner diameter, whose front face was at a 122 ± 2 mm distance from the jet target. Thus, the solid angle of this detector setup is $\Delta\Omega = (3.65 \pm 0.17) \times 10^{-7}$ sr. The observed yields provide information on the product of beam intensity (N_p) and target density (n_t) as well as on the purity of the target gas and of the ion beam. This method requires an a priori knowledge of the elastic scattering cross section (Sect. 3.2.1). The uncertainty in the detection angle θ_{lab} also enters critically in this method. From the geometrical arrangement in the target chamber (Fig. 1b), a value of $\theta_{lab} = 29.6° \pm 1.2°$ was found. A second determination involved the elastic scattering of 1 MeV protons on ^4He target nuclei, using the setup shown in Fig. 1 and the 4 MV Dynamitron tandem accelerator at the Ruhr-Universität Bochum [18]. In this case, the intensity of the elastic scattered projectiles (I_{sc}) and that of the recoil target nuclei (I_{rec}) were measured in the same detector at a nominal angle of 30°: $I_{sc}/I_{rec} = 2.89 \pm 0.15$. This intensity ratio depends sensitively on the detection angle θ_{lab}. Using the elastic scattering cross sections reported at 28°, 30°, and 33° [21], one arrives at $\theta_{lab} = 30.1° \pm 0.9°$. The weighted average (of this value with the geometrically determined value), $\theta_{lab} = 29.9° \pm 0.7°$, was adopted.

Alternatively, the beam intensity was measured by a 200 W beam calorimeter [22] placed at a distance of 161 ± 2 mm from the jet target (Fig. 1): the beam is stopped in the calorimeter, where the kinetic energy E_{lab} of the projectiles is converted into heat which is measured by the calorimeter. The total integrated beam power $L(t)$ at the calorimeter over a time period t yields the total number of incident ions $N_p(t)$ over this time period, $N_p(t) = L(t)/E_{lab}$. This method ignores the charge state of the incident ions and, when combined with an accurate energy determination of the incident projectiles (including the energy loss in the target gas), it gives an accurate determination of the number of incident ions in a given run. The problem of heat losses, e.g., via conduction and convection transport mechanisms, has been minimized in the design of a constant temperature gradient [22]. The 200 W calorimeter [22] allowed an absolute current determination to an accuracy of $\pm 3\%$ for beam powers above 15 W, where all measurements were carried out. The calorimeter was placed at such a distance from the jet target (Fig. 1) that angle straggling of the beam in the gas resulted in a beam profile smaller than the 200 mm^2 active area of the calorimeter.

2.2. Jet Target Density

The number of ^4He atoms per cm^2 in the jet target zone (N_t) was determined using several methods, which are discussed below. The adopted weighted average is $N_t = (3.51 \pm 0.16) \times 10^{17}$ atoms/cm^2 (external error $= \pm 0.11$) for $p_0 = 1.96$ bar.

2.2.1. Target Density via Rutherford Scattering. In this method the $^3He+^4He$ elastic scattering yield $I_{el}(\theta_{lab})$ was observed in the monitor counter at $\theta_{lab}=29.9°$,

$$I_{el}(\theta_{lab})=N_p\,N_t[d\sigma/d\Omega(\theta_{lab})]_{el}\,\Delta\Omega, \quad (3)$$

and the number of incident ^3He projectiles (N_p) was measured concurrently with the 200 W calorimeter. At $E(^3He)=352.2$ keV the $^3He+^4He$ elastic scattering cross section $[d\sigma/d\Omega(\theta_{lab})]_{el}$ follows the Rutherford scattering law (Sect. 3.2.1). For $p_0=1.96$ bar, the energy loss of the ^3He ion beam in the ^4He gas of the jet target chamber (Sect. 2.4) leads to an effective energy of the projectiles at the center of the jet target (or at the calorimeter) of $E_{eff}=342.9$ keV (or 336.6 keV). The measurement yields $N_t=(3.45\pm0.30)\times10^{17}$ atoms/cm^2. The quoted error was obtained by quadratic addition of uncertainties in I_{el}(2.0%), N_p(3.0%), $d\sigma/d\Omega$(6.5%), $\Delta\Omega$(4.7%) and the energy loss correction (1.5%).

2.2.2. Target Density via Mott Scattering. Similarly to the method just discussed, the $^4He+^4He$ elastic scattering at $E(^4He)=352.2$ keV ($E_{eff}=343.6$ keV at the center of the jet target, Sect. 2.4) was used to determine N_t. It is known [23, 24] that the elastic scattering yield at this energy follows the Mott scattering law to better than 2%. The measurements led to $N_t=(3.53\pm0.24)\times10^{17}$ atoms/cm^2 at $p_0=1.96$ bar, where the quoted uncertainty was obtained in a similar manner as discussed above.

2.2.3. Target Density via Energy Loss. Here, a ^{12}C target of 80 μg/cm^2 thickness (evaporated onto a 0.2 mm thick Ta backing) was placed at the 0° port of the target chamber (Fig. 1b) and the ground state γ-ray transition from the $^{12}C(p,\gamma)^{13}N$ reaction ($Q=1943.3\pm0.3$ keV, [19]) was observed at $\theta_\gamma=0°$ with the intrinsic Ge detector in close geometry. Due to the smooth yield curve of this reaction [25], the capture transition is observable at all beam energies of interest. A γ-ray spectrum was obtained at $E_p=352$ keV with no gas in the target chamber and the energy of the γ-ray transition was determined using room background lines as energy calibration standards: $E_\gamma=511.0$, 1460.8, 2614.6 keV. With ^4He gas of $p_0=1.96$ bar in the jet system, the incident beam loses energy over the distance from the aperture to the ^{12}C target and hence the γ-ray transition is shifted in energy by an amount equal to this energy loss: $\Delta_{lab}=4.30\pm0.17$ keV. This energy loss arises from the jet target zone as well as the ambient pressure in the target chamber ($p_t=0.49\pm0.03$ mbar). Using this pressure and stopping power tables [26], an energy loss of 2.72 ± 0.31 keV was calculated for the region outside the jet target zone, hence $\Delta_{jet}=1.58\pm0.19$ keV and $N_t=(3.99\pm0.54)\times10^{17}$ atoms/cm^2, where a 6% uncertainty in the stopping power value was included in the analysis.

2.2.4. Target Density via Jet Profile. The measurement of the radial density distribution $j(r)$ of the supersonic jet stream along the beam axis has been discussed in Sect. 2.1.3 and the results for ^4He gas at $p_0=1.96$ bar are shown in Fig. 2. The radial integral over this distribution (in relative units) can be expressed as

$$\int j(r)\,dr=l_{eff}(j_{max}-j_{min}),$$

where l_{eff} is the effective width of the jet distribution (defined by this expression) and j_{max} (and j_{min}) the maximum (and minimum) values of the distribution (Fig. 2). Numerical integration of the observed distribution together with the ratio $R=j_{max}/j_{min}=119\pm15$ (Fig. 2) leads to $l_{eff}=2.3\pm0.1$ mm, which is nearly identical with the FWHM width ($l_j=2.0\pm0.1$ mm). Since the quantity j_{min} corresponds to the ambient pressure in the target chamber ($p_t=0.49\pm0.03$ mbar, or $n_t=(1.20\pm0.06)\times10^{16}$ atoms/cm^3 for a gas temperature of 25° C), the above expression can be written in absolute units: $N_t=l_{eff}\,n_t\,R=(3.23\pm0.45)\times10^{17}$ atoms/cm^2.

2.3. Gamma-Ray Efficiency

Due to the lead shielding around the Ge detector (Fig. 1b), capture transitions are observed predominantly as created in the jet target zone. The absolute γ-ray efficiency, $\varepsilon_\gamma(E_\gamma,r)$, of the detector depends on the γ-ray energy E_γ and, for an extended gas target, on the distance r along the beam axis. The mean efficiency $\varepsilon_\gamma(E_\gamma)$ is then determined by weighting the efficiency $\varepsilon_\gamma(E_\gamma,r)$ with the jet profile density $j(r)$ (Fig. 2):

$$\varepsilon_\gamma(E_\gamma)=\int j(r)\,\varepsilon_\gamma(E_\gamma,r)\,dr/\int j(r)\,dr. \quad (4)$$

The efficiency $\varepsilon_\gamma(E_\gamma,r)$ was determined [18] for energies of $E_\gamma=0.30$ to 1.33 MeV using calibrated sources (^{22}Na, ^{60}Co, ^{133}Ba and ^{137}Cs) over a distance of −16 cm to +16 cm around the jet target. The integrals in equation 4 were numerically evaluated; an integration step of 0.1 mm was found to be sufficient. The results showed that the values for $\varepsilon_\gamma(E_\gamma)$ and $\varepsilon_\gamma(E_\gamma,r=0)$ were nearly identical (e.g., a 0.64% difference at $E_\gamma\leqq1$ MeV). Thus, the $\varepsilon_\gamma(E_\gamma,r=0)$ values have been adopted for the mean absolute efficiency of the Ge detector.

In a second experiment the well known $^{14}N(p,\gamma)^{15}O$ resonance at $E_R=278$ keV [27] was

used [18] to extend the $\varepsilon_\gamma(E_\gamma)$ values up to $E_\gamma = 2.37$ MeV. The results were in excellent agreement with the radioactive source values in the overlapping energy range, and yield the relation $\varepsilon_\gamma(E_\gamma) = 0.59\, E_\gamma^{-0.75}$ (E_γ in keV), with an error of $\pm 4.5\%$.

2.4. Effective Beam Energy

Due to the energy loss of the ^3He beam in the target gas ($p_0 = 1.96$ bar), the effective beam energy E_{eff} at, say, the center of the jet target is related to the incident projectile energy ($E_{lab} = 352.2 \pm 0.3$ keV) by

$$E_{eff}(\text{jet}) = E_{lab} - \Delta E_1 - \Delta E_{jet}/2,$$

where $\Delta E_1 = 6.4 \pm 0.7$ keV is the energy loss of the beam over the distance from the aperture to the jet target (ambient pressure $p_t = 0.49 \pm 0.03$ mbar, distance $= 31.0 \pm 0.2$ cm) and $\Delta E_{jet} = 5.9 \pm 0.6$ keV (Sect. 2.2); thus $E_{eff}(\text{jet}) = 342.9 \pm 1.0$ keV, or, in the center-of-mass system, $E(\text{jet}) = 195.5 \pm 0.6$ keV. At the position of the calorimeter, one finds in an analogous way

$$E_{eff}(\text{cal}) = E_{lab} - \Delta E_1 - \Delta E_{jet} - \Delta E_2 = 336.6 \pm 1.0 \text{ keV}.$$

Due to the non-resonant nature of the $^3He(\alpha,\gamma)^7Be$ reaction, the two primary γ-ray transitions (DC $\rightarrow$ 0 and DC $\rightarrow$ 429.1 keV) can be observed at all beam energies and their energies change with beam energy according to the relation

$$E_\gamma(\text{DC} \rightarrow E_x) = Q + E - E_x.$$

With the Q-value of 1586.7 ± 0.6 keV (weighted average of values quoted by [9] and [28]) the energies of the capture transitions fall in a region where comparison with the precisely known energies of γ-rays from radioactive sources or room background is possible (Sect. 2.2.3). For the conditions $E_{lab} = 352.2$ keV and $p_0 = 1.96$ bar, this method led to an effective energy $E(\text{jet}) = 195.1 \pm 0.9$ keV, in excellent agreement with the above value. The weighted average, $E(\text{jet}) = 195.4 \pm 0.5$ keV, has been adopted.

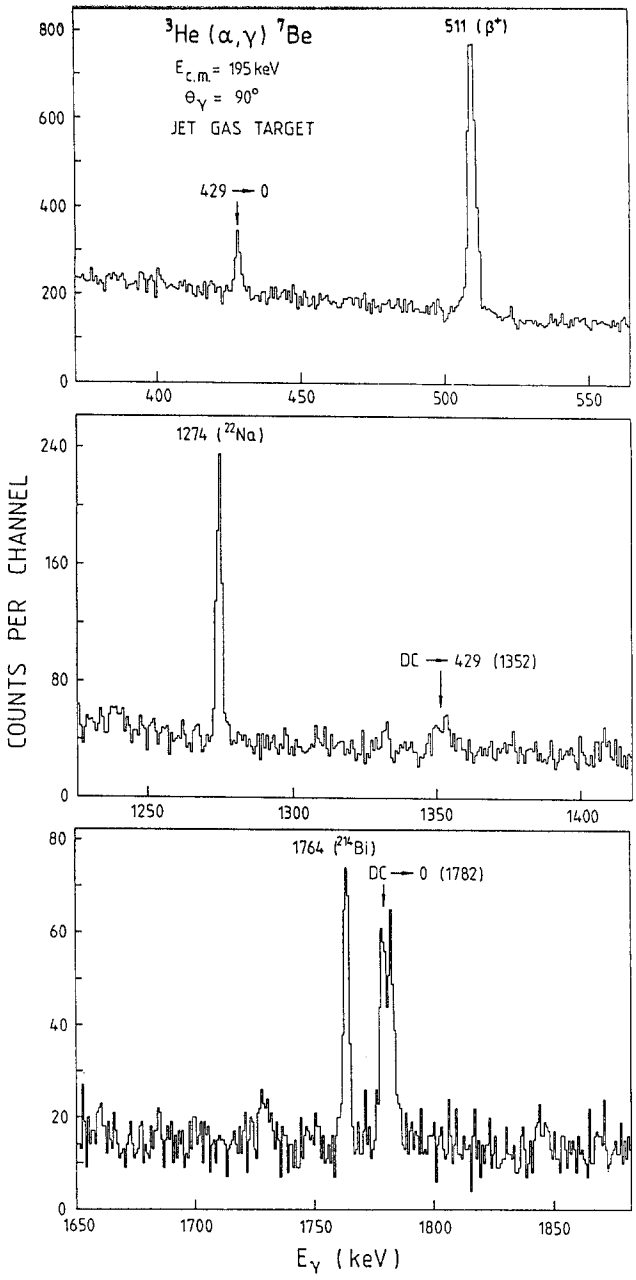

Fig. 3. Relevant sections of the γ-ray spectrum obtained with the intrinsic Ge detector in the jet target setup (Fig. 1) for an accumulated charge of 5.7 C

2.5. Absolute Cross Section

Relevant sections of the γ-ray spectrum obtained with the intrinsic Ge detector at $E_{lab} = 352.2$ keV ($E(\text{jet}) = 195.4 \pm 0.5$ keV) are shown in Fig. 3. The observed counts in the 429 $\rightarrow$ 0, DC $\rightarrow$ 429 and DC $\rightarrow$ 0 keV capture transitions, corrected for γ-ray efficiency (Sect. 2.3) and angular distribution effects [6, 9], led to a total yield for the two primary transitions of $Y_{tot} = 2.26 \times 10^5 (\pm 8.2\%)$, where Y_{tot} is related to (2) by

$$Y_{tot} = I_\gamma(E)/[l_{eff}\, \varepsilon_\gamma\, W(\theta_\gamma, E)]. \quad (5)$$

The number of incident ^3He nuclei during this run of 22.2 h, as observed with the calorimeter, was $N_p = 3.56 \times 10^{19} (\pm 3\%)$. With the relation

$$Y_{tot} = N_p\, n_t\, \sigma(E), \quad (6)$$

and $N_t = n_t l_{eff} = 3.51 \times 10^{17} (\pm 4.6\%)$ atoms/cm^2 (Sect. 2.2), one finds a cross section of $\sigma(E) = 18.1 \pm 1.8$ nb at $E = 195.4$ keV. The $^3He + ^4He$ elastic scattering yield was concurrently observed in the 29.9° monitor counter (Sect. 2.1.4), leading to $\sigma(E) = 18.4 \pm 2.2$ nb. Taking into account common uncertainties in the two values, one arrives at a weighted average of $\sigma(E) = 18.2 \pm 1.7$ nb, or $S(E) = 0.45 \pm 0.04$ keV-*b*. Note that the ± 0.5 keV uncertainty in E contributes very little ($\pm 1.3\%$) to the quoted error for $S(E)$.

3. Measurements Using the Extended Gas Target

3.1. Experimental Equipment and Setup

3.1.1. Accelerator. The 4 MV Dynamitron accelerator at the Institut für Strahlenphysik in Stuttgart provided a $^4He^+$ beam at energies $E_\alpha = 0.8$ to 1.6 MeV, with particle currents of up to 90 μA at the target. Details of the accelerator, the beam handling system, and the beam characteristics have been described previously [29].

3.1.2. Extended Gas Target System and Setup. Here, a gas target system of four pumping stages was used [30]. A schematic diagram of the relevant parts of the system and of the experimental setup is shown in Fig. 4. The beam enters the disk-shaped target chamber (20 cm diameter, 3 cm height; central pipe of 2 cm diameter) through five Ta apertures (*A* to *E*) and is stopped in the 200 W calorimeter (Sect. 2.1.4) at a distance of 40.6 ± 0.3 cm from the aperture *A*. The chamber has several ports radiating from the center of the chamber; the center is at a distance of 9.9 ± 0.1 cm from the aperture *A*. These ports are used for several purposes (Fig. 4a). The gas pressure in the target chamber, p_t, was measured with a Baratron capacitance manometer to an accuracy of $\pm 4\%$. Reduction of gas pressure along the beam axis, due to beam induced heating, is less than 8% for the maximum 5.3 mbar ^3He target pressure used and the 90 μA maximum beam current employed (for details, see [31]). The gas pressure at several other locations in the gas target system was determined by thermocouple, Penning and ionization manometers [30]. For ^3He gas (99.9% enriched in ^3He) of $p_t = 2.7$ mbar pressure in the target chamber, the four-stage pumping system reduced the pressure to 3×10^{-2} and 1×10^{-6} mbar in the regions between the apertures *A* and *B* and *D* and *E*, respectively (Fig. 4a). A similar pressure reduction was observed for other p_t values. The gas composition was monitored with the *Q* 200 mass spectrometer [30]. The zeolite adsorption trap (Sect. 2.1.2) was used for the cleaning of the ^3He target gas.

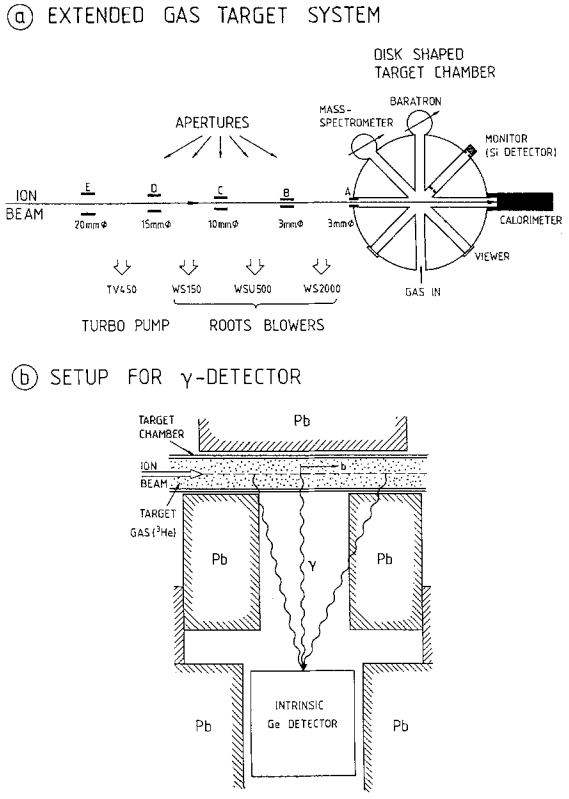

Fig. 4a and b. Shown schematically are relevant parts of **a** the extended gas target system and **b** the arrangement used for γ-ray spectroscopy. The beam enters the disk-shaped target chamber through a 3 mm diameter aperture (*A*) and is stopped in the beam calorimeter. The effective target length seen by the intrinsic Ge detector is defined here by the lead collimator; the parameter *b*, shown in the figure and in Fig. 6a, is distance along the beam axis, measured from the center of the target chamber

The $^3He + ^4He$ elastic scattering yield was observed with a Si detector (100 μm thickness, 300 mm^2 active area) placed at $\theta_{lab} = 45°$ (Fig. 4a).

The capture γ-rays from $^3He(\alpha,\gamma)^7Be$ were observed with an 85 cm^3 intrinsic Ge detector. The energy resolution (in the setup) was 2.1 keV at $E_\gamma = 1.33$ MeV. The detector was placed at $\theta_\gamma = 90°$ and at a distance of 11.9 ± 0.2 cm from the beam axis (Fig. 4b). In this setup, the target volume is extended from the aperture *A* to the beam stop. Therefore, the effective length l_{eff} seen by the Ge detector was defined by lead shielding around the detector (Fig. 4b). In front of the detector was a cylindrical lead collimator (8.7 cm length, 6.0 cm inner diameter, 4.0 cm wall thickness). At other places, the lead shielding was 5 to 10 cm thick.

3.2. Experimental Procedures and Results

As described in Sect. 2.4, the effective center-of-mass energy E for each run (Table 1) was determined via the energies of the DC → 0 and DC → 429 keV primary γ-ray transitions. Furthermore, the number of ^3He target atoms per cm^3, n_t, was calculated (Table 1) from the gas pressure in the target chamber ($\pm 4\%$), corrected for the gas temperature of $25 \pm 5°$ C, and the number of incident ^4He projectiles, N_p, was obtained (Table 1) via the 200 W calorimeter (Sect. 2.1.4).

3.2.1. Elastic Scattering Yield. From the $^3He+^4He$ elastic scattering yield, $I_{el}(\theta_{lab})$, observed at $\theta_{lab}=45°$ (Sect. 3.1.2), one obtains information on the product $N_p N_t$ via an expression similar to (3):

$$I_{el}(\theta_{lab}) = N_p N_t \, l \, \Delta\Omega [d\sigma/d\Omega(\theta_{lab})]_{el}. \quad (7)$$

The Si detector was collimated by a circular aperture of 3.030 ± 0.005 mm diameter and a slit aperture of 1.020 ± 0.005 mm width (both determined with a microscope) placed at respective distances to the center of the chamber of 175.6 ± 0.5 mm and 27.0 ± 0.5 mm. The detector views a horizontal length of $l = 1.70$ mm of the extended gas target, leading to the product $l \times \Delta\Omega = (3.99 \pm 0.06) \times 10^{-5}$ cm − sr. In another run, the circular aperture had a diameter of 0.525 ± 0.005 mm, thus $l \times \Delta\Omega = (1.20 \pm 0.05) \times 10^{-6}$ cm-sr.

In order to determine the deviations of the elastic scattering cross section, $[d\sigma/d\Omega(\theta_{lab})]_{el}$, from the Rutherford scattering law, argon gas of natural isotopic composition was admixed into the ^3He target gas. It is known [32] that the $^4He+^{40}Ar$ elastic scattering yield at $E_\alpha \leqq 3.0$ MeV follows the Rutherford scattering law. The energy dependence of the $^3He+^4He$ elastic scattering yield relative to argon is shown in Fig. 5. The results have been normalized to Rutherford scattering at the lowest energies, where the intensity ratio approached a constant value. Using these data together with the intensity ratio of the elastically scattered projectiles and the recoil target nuclei, one finds the actual detector angle to be $\theta_{lab} = 45.4 \pm 0.3°$. The resulting values for $N_p n_t$ (Table 1) have an error of $\pm 2.3\%$ and are consistent with the

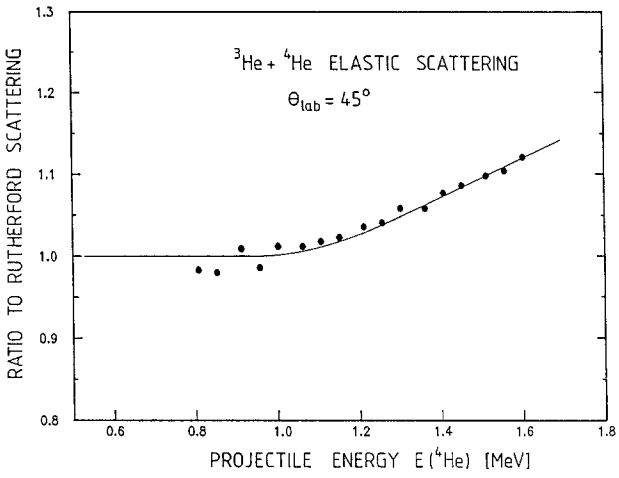

Fig. 5. The observed energy dependence of the elastic scattering yields for the $^3He+^4He$ system is shown relative to the Rutherford scattering law at the angle of $\theta_{lab}=45°$. The data have been normalized to Rutherford scattering at the lowest energies. The curve through the data points is to guide the eye

Table 1. Summary of results using the extended gas target

E[a] (keV)	n_t[b]	N_p[c]	$N_p n_t$ ($\times 10^{36}/cm^3$) [d]	[e]	[f]	Y_{tot}[h] (10^5/cm)	$\sigma(E)$ (μb)	$S(E)$[i] (keV-b)
437.7	5.90	2.31	1.36	1.58	1.50 ± 0.04[g]	5.7 ± 0.5	0.38 ± 0.04	0.43 ± 0.05
547.1	6.73	1.41	0.77	0.75	0.76 ± 0.02	4.7 ± 0.4	0.62 ± 0.06	0.38 ± 0.04
662.8	6.88	0.493	0.34	0.34	0.34 ± 0.01	3.2 ± 0.3	0.92 ± 0.09	0.36 ± 0.04
664.5	12.0	0.699	0.84	0.86	0.85 ± 0.02	7.7 ± 0.7	0.91 ± 0.08	0.35 ± 0.03

[a] Center of mass energy calculated from the energies of the DC → 0 and DC → 429 keV transitions in $^3He(\alpha,\gamma)^7Be$. The E values have an error of ± 1.0 keV arising predominantly from the uncertainties in the energy calibration of the Ge(Li) detector ($= \pm 0.8$ keV)
[b] Number of target atoms (in units of $10^{16}/cm^3$) as deduced from the gas pressure including corrections for beam-induced effects [31]: overall error $= \pm 2\%$
[c] Number of projectiles (beam particles) (in units of 10^{19}) as deduced from the 200 W calorimeter with an overall error of $\pm 3\%$
[d] From columns 2 and 3 with an overall error of $\pm 3.6\%$
[e] From elastic scattering yields, with an overall error of $\pm 2.3\%$
[f] Weighted average with internal error (external error $= \pm 0.7\%$ to $\pm 2.9\%$)
[g] External error (internal error $= \pm 1.9\%$)
[h] Y_{tot} (5) as deduced from the DC → 0 primary transition plus the weighted average of the DC → 429 → 0 keV $\gamma\gamma$ cascade
[i] Quoted error includes the uncertainty in E (column 1)

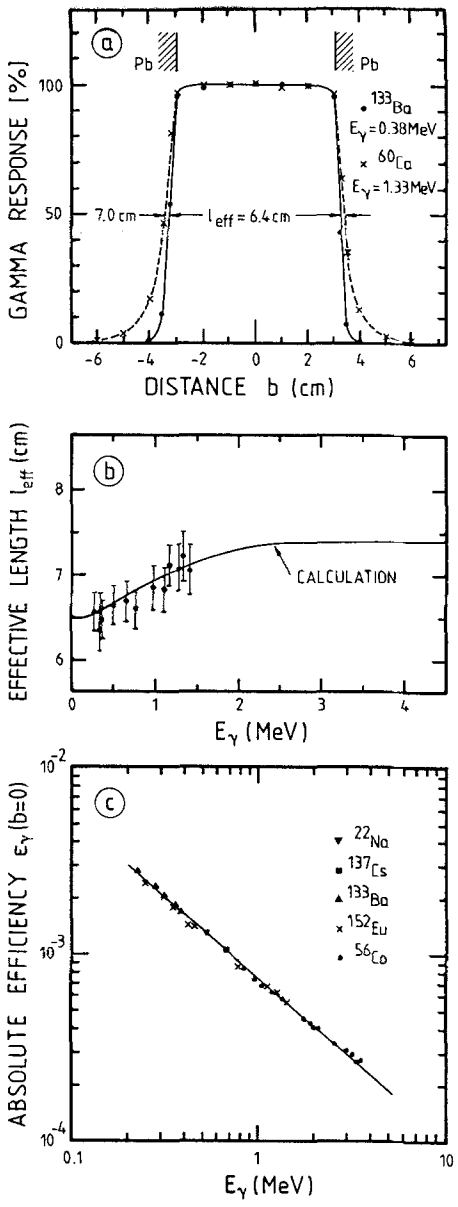

Fig. 6. a Response function of the Ge detector for two γ-ray energies in the setup shown in Fig. 4b. The response function is flat to $\pm 2\%$ within the lead collimator and drops steeply when the sources are placed near and beyond the shielding. The curves through the data points are to guide the eye. **b** The effective target length l_{eff} in this setup varies slightly with γ-ray energy. The observed and calculated values are in good agreement. **c** The absolute γ-ray efficiency at the center of the target chamber ($b=0$) is shown. The straight line through the data points is given by the expression $\varepsilon_\gamma = 0.28\, E_\gamma^{-0.86}$ (E_γ in keV)

other measurements. The weighted-average values (Table 1) have been adopted.

3.2.2. Gamma-ray Efficiency in the Setup. As discussed in Sect. 3.1.2, the effective target length l_{eff} seen by the γ-ray detector is defined by the lead shielding

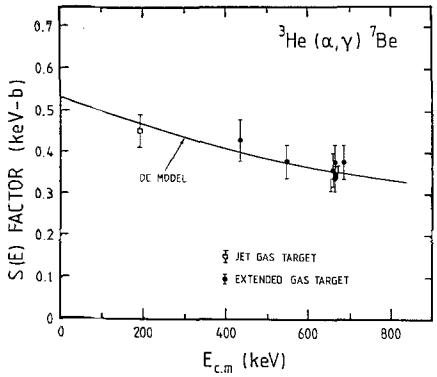

Fig. 7. Experimental results for the $^3He(\alpha,\gamma)^7Be$ astrophysical $S(E)$ factor as obtained from the γ-ray measurements of the present work. The $S(E)$ values obtained from the activation method differ by the factors given in Table 2. The solid curve is the DC model prediction [6] normalized to the γ-ray data

around the detector. Due to this shielding and solid angle effects of the Ge detector, the length l_{eff} also depends on γ-ray energy. The length l_{eff} was determined with radioactive sources, which were moved along the beam axis within the target chamber (Fig. 6a). The observed and calculated target lengths l_{eff} are shown in Fig. 6b as a function of γ-ray energy. One sees that l_{eff} has a lower limit as defined by the geometry of the setup and approaches a maximum value for $E_\gamma \geqq 2$ MeV. Thus, the effective target length l_{eff} is known to an estimated precision of $\Delta l_{eff}/l_{eff} = \pm 5\%$. The absolute detection efficiency ε_γ at the distance $b=0$ (Fig. 6a) was determined with calibrated γ-ray sources ($E_\gamma = 0.2$ to 3.5 MeV; Fig. 6c), placed at the center of the target chamber, to an estimated accuracy of $\Delta\varepsilon_\gamma/\varepsilon_\gamma = \pm 4\%$. The product $l_{eff}\,\varepsilon_\gamma$ is thus known to an accuracy of $\pm 7\%$.

3.2.3. Absolute Cross Sections. All measurements led to a branching ratio of $R = I(\mathrm{DC}\to 429)/I(\mathrm{DC}\to 0) = 0.45 \pm 0.02$, in good agreement with previous work ($R = 0.43 \pm 0.02$, [9]). Using the values for Y_{tot} and $N_p\, n_t$ (Table 1) and (6), the resulting absolute cross sections $\sigma(E)$ are summarized in Table 1 and the corresponding $S(E)$-factor values (1) are displayed in Fig. 7.

4. Concurrent Measurement of Capture γ-Rays and ^{7}Be Activity

In the $^3He(\alpha,\gamma)^7Be$ reaction the DC $\to 0$ plus DC $\to 429$ keV capture γ-rays and the ^{7}Be residual nuclei are produced in equal numbers, where the ^{7}Be nuclei can be detected via their electron-capture decay to the 478 keV state in ^{7}Li ($T_{1/2} = 53.29 \pm 0.07\,d$ [33]; branching ratio $= 10.45 \pm 0.04\%$ [34]). For such a concurrent measurement of both reaction products,

Table 2. Concurrent measurement of capture γ-rays and ^7Be activity

Run[a] #	E[b] (keV)	I[c] (μA)	$N_p n_t$[d] (10^{36}/cm^3)	Y_{tot}[e] (10^6/cm)	$\sigma(\gamma, E)$ (μb)	$I(^7Be)$ (10^7)	$\sigma(^7Be, E)/\sigma(\gamma, E)$
1	685.8	17	0.97	1.01 ± 0.09	1.04 ± 0.09	3.7 ± 0.5	1.9 ± 0.3
2	664.4	47	2.50	2.22 ± 0.18	0.89 ± 0.07	6.8 ± 1.2	1.5 ± 0.3
3	664.8	53	2.38	2.12 ± 0.17	0.89 ± 0.07	6.4 ± 0.5	1.5 ± 0.2
4	666.4	92	3.06	3.02 ± 0.26	0.99 ± 0.09	5.1 ± 0.5	0.9 ± 0.1

[a] The target pressure in these runs was 5.1 to 5.3 mbar. The runs are ordered with respect to increasing beam current on target (column 3)
[b] Center-of-mass energies with an error of ±1.0 keV (for details, see footnote[a] in Table 1)
[c] ^4He current in the target chamber
[d] From elastic scattering yields, with an overall error of $\pm2.3\%$
[e] See footnote [h] of Table 1

the prompt capture γ-rays were observed during the ^7Be activation and then compared with the number of ^7Be nuclei produced, as obtained subsequently via the 478 keV γ-ray activity of ^7Be. For these measurements, the extended gas target setup (Fig. 4) was used, except that the 200 W calorimeter was replaced by a watercooled Ta backing (placed at a distance of 19.8 ± 0.1 cm from the center of the aperture A).

The analysis of 4 runs at center-of-mass energies $E=664$ to 686 keV for the capture γ-rays is identical to that described in Sect. 3, except that the product $N_p N_t$ was obtained here alone from the $^3He+^4He$ elastic scattering yields. The results are summarized in Table 2 and are in good agreement with the other measurements (Table 1 and Fig. 7).

Since the ^7Be residual nuclei, produced concurrently in these runs, are moving essentially in the beam direction, they should be implanted in the Ta backing. Each ^7Be-implanted Ta backing was positioned in close geometry to an 80 cm^3 Ge(Li) detector (typical distance = 4.5 cm), which was surrounded by a 5 cm thick lead shield to suppress room background. The detector γ-ray efficiency ε_γ was determined with calibrated sources to an accuracy of $\pm5\%$. The ^7Be activity of each Ta backing was observed over a time period of up to 97 days, during which the 478 keV γ-ray activity decreased accordingly to the known ^7Be halflife. After taking into account the γ-ray efficiency, the 10.45% branching ratio in the ^7Be decay and the ^7Be halflife, the numbers of ^7Be residual nuclei, $I(^7Be)$, produced in each run are listed in Table 2.

In order to check a possible loss of ^7Be nuclei from the implanted Ta backing, caused e.g. by sputtering by the incident α-beam, the wall of the central pipe of the disk-shaped target chamber was covered in run 2 (Table 2) with a 0.05 mm thick Al foil. At the end of the run, this catcher foil was folded and placed in front of the Ge(Li) detector, yielding an upper limit of 3% for a possible ^7Be loss, consistent with previous observations [34].

Since the activation times t_a were of the order of 1 day, and $\lambda t_a = \ln 2 \times t_a/T_{1/2} = 0.013$, corrections arising from the ^7Be decay during activation are less than 1%, and thus the yield $I(^7Be)$ is related to the cross section to good approximation by the relation

$$I(^7Be) = N_p n_t l_{eff*} \sigma(E), \tag{8}$$

where $l_{eff*} = 19.8\pm0.1$ cm is here the gas target length from the aperture A to the Ta backing. Combining (2) and (8) leads to the ratio

$$I(^7Be), E)/I_\gamma(E) = [l_{eff*}/l_{eff}\,\varepsilon_\gamma\, W(\theta_\gamma, E)] \cdot [\sigma(^7Be, E)/\sigma(\gamma, E)], \tag{9}$$

which is independent of the product $N_p n_t$. The resulting ratios $X = \sigma(^7Be, E)/\sigma(\gamma, E)$ are summarized in Table 2. While one expects a ratio of unity (or slightly less than one due to ^7Be losses), the observed values are on the average higher than unity (weighted average $X = 1.1\pm0.2$), where the deviations from unity appear to decrease with increasing beam current (Table 2).

In order to find possible causes of this disagreement, several tests have been carried out [18].

(i) Comparison of the yield of the ^{40}K background line ($E_\gamma = 1460$ keV), observed during the runs and off-line, showed that dead time effects in the capture γ-ray detection were negligible ($\leqq0.5\%$).

(ii) The γ-ray production yield along the beam axis of the extended target chamber (Fig. 4) was investigated wilth a second Ge(Li) detector (80 cm^3) placed on the opposite side of the disk-shaped target chamber at $\theta_\gamma = 90°$ and at a distance of 11.6 ± 0.1 cm from the beam axis. With lead collimators in front of the detector, the detector viewed a 6.0 cm long section of the target volume. The γ-ray yields observed near the aperture A at the entrance of the chamber, near the center of the chamber and near the Ta backing were identical within $\pm5\%$ (normalized to elastic scattering yields).

(iii) The gas pressure in the target chamber was

measured near the beam stop and found to be identical (within $\pm 1\%$) with the value observed at the center.

These tests showed that the cause of the deviation of the ratio from unity is probably not to be found in the parameters relevant to the $^3He(\alpha,\gamma)^7Be$ reaction. In principle, impurities in the $^4He^+$ ion beam (e.g., DH_2^+) and in the Ta implantation backing (e.g., ^6Li and ^{10}B) could cause additional production of ^7Be nuclei by such reactions as $^6Li(p,\gamma)^7Be$, $^6Li(d,n)^7Be$ and $^{10}B(p,\alpha)^7Be$. With $\sigma(E) \cong 1\ \mu b$ for $^3He(\alpha,\gamma)^7Be$ at $E_\alpha = 1.6$ MeV (Table 2), and $\sigma(E) \cong 40$ mb for $^{10}B(p,\alpha)^7Be$ at $E_p = 0.4$ MeV [35, 36] (DH_2^+ beam), the ratio could be explained if the product $N_p n_t$ for $^{10}B(p,\alpha)^7Be$ is only 5×10^{-6} times that of the $^3He(\alpha,\gamma)^7Be$ reaction. Quantitative measurement and control of such small impurities in both the ion beam and the target material is extremely difficult. Because such measurements were not carried out in the course of the irradiations, the values of the absolute cross section as deduced from the activity method represent only an upper limit on the true value ($X \leqq 1.3$, or $S(0) \leqq 0.69$ keV-*b*).

5. Discussion

The absolute $S(E)$ factors as deduced from the prompt capture γ-ray transitions (Tables 1 and 2) are displayed in Fig. 7 together with the DC model calculations fitted to the data. The resulting $S(0)$ value of 0.53 ± 0.03 keV-*b* is in good agreement with previous work (Table 3) leading to a weighted average of $S(0) = 0.51 \pm 0.02$ keV-*b*. The determinations by measurement of the induced ^7Be activity are also consistent with each other, but lead to a weighted average of $S(0) = 0.58 \pm 0.02$ keV-*b* (Table 3), a value three and a half standard deviations different. Because the various activation method results shown in Table 3 were obtained at different energies, on different types of accelerator (one-stage or tandem accelerators), and with different implantation targets, it would be reasonable to expect substantial differences in the production of ^7Be by contaminant reactions. However, statistical considerations make a definitive statement impossible with the data in hand at this time. We recommend therefore the value $S(0) = 0.51 \pm 0.02$ keV-*b*, which is only slightly below the value of 0.52 keV-*b* chosen by Bahcall et al. [2] to calculate the expected solar neutrino flux.

Table 3. $S(0)$ values for $^3He(\alpha,\gamma)^7Be$ from previous and present work

$S(0)$[a] (keV-*b*)	Reference
Method: *prompt capture γ-rays transitions*	
0.47 ± 0.05	Parker and Kavanagh (1963) [5]
0.58 ± 0.07[b]	Nagatani et al. (1969) [7]
0.45 ± 0.06[c]	Kräwinkel et al. (1982) [9]
0.52 ± 0.03	Osborne et al. (1982) [10]
0.47 ± 0.04	Alexander et al. (1984) [13]
0.53 ± 0.03[d]	Present work
0.51 ± 0.02	Weighted average
Method: ^7Be *activity*	
0.55 ± 0.05	Osborne et al. (1982) [10]
0.63 ± 0.04	Robertson et al. (1983) [11]
0.56 ± 0.03	Volk et al. (1983) [12]
$\leqq 0.69$[e]	Present work
0.58 ± 0.02	Weighted average

[a] The DC model prediction for the energy dependence of $S(E)$ [6] was used in the extrapolation of the data to zero energy

[b] Result of reanalysis [4, 8]; $S(0) = 0.61 \pm 0.07$ keV-*b* as reported originally

[c] Result based only on jet density as measured via elastic scattering yields (Sect. 1); $S(0) = 0.32 \pm 0.04$ keV-*b* as reported originally

[d] From Fig. 7 and Tables 1 and 2

[e] Section 4, not included in the weighted average

The authors would like to thank K. Brehm, H. Ebbing, S. Engstler, G. Ganteför, A. Gardberg, U. Giesen, J. Görres, V. Harms, U. Heinemann, M. Köster, A. Krauss, R. Plaga, A. Redder, S. Schmidt, U. Schröder, S. Seuthe, R. Timmermann, K. Wolke and S. Wüstenbecker for useful discussions as well as for assistance during the course of the experiments. Fruitful comments on the manuscript by Prof. C.A. Barnes (Caltech) are highly appreciated.

References

1. Bahcall, J.N., Davis, R.: Essays in nuclear astrophysics. Barnes, C.A., Clayton, D.D., Schramm, D.N. (eds.), p. 243. Cambridge: Cambridge University Press 1982
2. Bahcall, J.N., Huebner, W.F., Lubow, S.H., Parker, P.D., Ulrich, R.K.: Rev. Mod. Phys. **54**, 767 (1982)
3. Bahcall, J.N., Cleveland, B.T., Davis, R., Rowley, J.K.: Astrophys. J. **292**, L 79 (1985)
4. Parker, P.D.: Physics of the sun. Sturrock, P.A. (ed.), p. 15. Dordrecht: Reidel 1985
5. Parker, P.D., Kavanagh, R.W.: Phys. Rev. **131**, 2578 (1963)
6. Tombrello, T.A., Parker, P.D.: Phys. Rev. **131**, 2582 (1963)
7. Nagatani, K., Dwarakanath, M.R., Ashery, D.: Nucl. Phys. A **128**, 325 (1969)
8. Kavanagh, R.W.: Essays in nuclear astrophysics. Barnes, C.A., Clayton, D.D., Schramm, D.N. (eds.), p. 159. Cambridge: Cambridge University Press 1982
9. Kräwinkel, H., Becker, H.W., Buchmann, L., Görres, J., Kettner, K.U., Kieser, W.E., Santo, R., Schmalbrock, P., Trautvetter, H.P., Vlieks, A., Rolfs, C., Hammer, J.W., Azuma, R.E., Rodney, W.S.: Z. Phys. A – Atoms and Nuclei **304**, 307 (1982)
10. Osborne, J.L., Barnes, C.A., Kavanagh, R.W., Kremer, R.M., Mathews, G.J., Zyskind, J.L., Parker, P.D., Howard, A.J.: Phys. Rev. Lett. **48**, 1664 (1982); Nucl. Phys. A **419**, 115 (1984)
11. Robertson, R.G.H., Dyer, P., Bowles, T.J., Brown, R.E., Jarmie, N., Maggiore, C.J., Austin, S.M.: Phys. REv. C **27**, 11 (1983)
12. Volk, H., Kräwinkel, H., Santo, R., Wallek, L.: Z. Phys. A – Atoms and Nuclei **310**, 91 (1983)
13. Alexander, T.K., Ball, G.C., Lennard, W.N., Geissel, H., Mak, H.B.: Nucl. Phys. A **427**, 526 (1984)

14. Becker, H.W., Buchmann, L., Görres, J., Kettner, K.U., Kräwinkel, H., Rolfs, C., Schmalbrock, P., Trautvetter, H.P., Vlieks, A.: Nucl. Instrum. Methods **198**, 277 (1982)
15. Redder, A., Becker, H.W., Lorenz-Wirzba, H., Rolfs, C., Schmalbrock, P., Trautvetter, H.P.: Z. Phys. A – Atoms and Nuclei **305**, 325 (1982)
16. Krauss, A., Becker, H.W., Trautvetter, H.P., Rolfs, C., Brand, K.: Nucl. Phys. A**465**, 150 (1987)
17. Krauss, A., Becker, H.W., Trautvetter, H.P., Rolfs, C.: Nucl. Phys. A**467**, 273 (1987)
18. Hilgemeier, M.: Thesis, Universität Münster (1987); Trautvetter, H.P.: Habilitationsschrift, Universität Münster (1984)
19. Freye, T., Lorenz-Wirzba, H., Cleff, B., Trautvetter, H.P., Rolfs, C.: Z. Phys. A**281**, 211 (1977)
20. Görres, J., Becker, H.W., Krauss, A., Redder, A., Rolfs, C., Trautvetter, H.P.: Nucl. Instrum. Methods A**241**, 334 (1985)
21. Kraus, L., Linck, I.: Nucl. Phys. A**224**, 45 (1974)
22. Vlieks, A., Hilgemeier, M., Rolfs, C.: Nucl. Instrum. Methods **213**, 291 (1983)
23. Heydenburg, N.P., Temmer, G.M.: Phys. Rev. **104**, 123 (1956)
24. Benn, J., Dally, E.B., Müller, H.H., Pixley, R.E., Staub, H.H., Winkler, H.: Nucl. Phys. A**106**, 296 (1968)
25. Rolfs, C., Azuma, R.E.: Nucl. Phys. A**227**, 291 (1974)
26. Andersen, H.H., Ziegler, J.F.: Hydrogen stopping powers and ranges in all elements. New York: Pergamon Press 1977; Ziegler, J.F.: Helium stopping powers and ranges in all elemental matter. New York: Pergamon Press 1977
27. Ajzenberg-Selove, F.: Nucl. Phys. A**449**, 1 (1986)
28. Wapstra, A.H., Audi, G.: Nucl. Phys. A**432**, 1, 55 (1985)
29. Hammer, J.W., Fischer, B., Hollick, H., Trautvetter, H.P., Kettner, K.U., Rolfs, C., Wiescher, M.: Nucl. Instrum. Methods **161**, 189 (1979)
30. Rolfs, C., Görres, J., Kettner, K.U., Lorenz-Wirzba, H., Schmalbrock, P., Trautvetter, H.P., Verhoeven, W.: Nucl. Instrum. Methods **157**, 19 (1978)
31. Görres, J., Kettner, K.U., Kräwinkel, H., Rolfs, C.: Nucl. Instrum. Methods **177**, 295 (1980)
32. Endt, P.M., Van der Leun, C.: Nucl. Phys. A**310**, 1 (1978)
33. Ajzenberg-Selove, F.: Nucl. Phys. A**413**, 1 (1984)
34. Skelton, R.T., Kavanagh, R.W.: Nucl. Phys. A**414**, 141 (1984)
35. Szabo, J., Csikai, J., Varnagy, M.: Nucl. Phys. A**195**, 527 (1972)
36. Cronin, J.W.: Phys. Rev. **101**, 298 (1956)

M. Hilgemeier, H.W. Becker, C. Rolfs, H.P. Trautvetter
Institut für Kernphysik
Universität Münster
Wilhelm-Klemm-Strasse 9
D-4400 Münster
Federal Republic of Germany

J.W. Hammer
Institut für Strahlenphysik
Universität Stuttgart
Pfaffenwaldring 58
D-7000 Stuttgart 80
Federal Republic of Germany